Thermochimica Acta, 53 (1982) 175–182
Elsevier Scientific Publishing Company, Amsterdam—Printed in The Netherlands

STRUCTURAL AND PHASE CHANGES IN IRON(III)–ALUMINIUM(III) MIXED HYDROXIDE–OXIDE SYSTEM: A THERMOANALYTICAL STUDY

B. MANI

Materials Science and Engineering, University of Pennsylvania, Philadelphia, PA 19104 (U.S.A.)

V. SITAKARA RAO

Chemistry Department, Indian Institute of Technology, Kharagpur-2 (India)

(Received 10 August 1981)

ABSTRACT

The structural and phase changes occurring in the ferric hydroxide gel, alumina gel and the coprecipitated ferric–aluminium hydroxide–oxide system are studied by thermoanalytical and X-ray diffraction techniques. The conversion of hydrated ferric oxide to hematite takes place through γ-Fe_2O_3 and alumina gel to oxide occurs through hydrargellite, bohemite as intermediate. The occurrence of solid solutions below 10 mole % of alumina, i.e. interstitial solid solution up to 1.5 mole %, then substitutional solid solution up to 3.43 mole % and thereafter separation of phases is observed. For higher concentrations of alumina, zones enriched in either hydrated iron oxide or aluminium oxyhydroxide are noticed.

INTRODUCTION

Magnetic dilution is an important method for determining the fundamental interaction between magnetic atoms and the value of the magnetic moments of such atoms [1]. The effect of this dilution on the magnetic properties of ferric oxide by a diamagnetic material such as aluminium oxide up to 10 mole % was studied in mixed oxides, sintered at 1000°C, using X-ray diffraction and Mössbauer spectroscopic measurements [2,3]. A similar type of dilution was attempted in our laboratory by the coprecipitation technique for Mössbauer spectroscopic investigations, electrical conductivity measurements and catalytic studies of these mixed hydroxides or oxides [4–6], as these are found to be efficient dehydration and dehydrogenation [7] and polymerization catalysts [8]. X-Ray diffraction, differential thermal analysis and thermogravimetric analysis were used to understand the phase and structural changes taking place during the dehydration and calcination of these hydroxides to oxides. The results are presented in this paper.

EXPERIMENTAL

Iron–aluminium mixed hydroxides with varying concentrations of aluminium hydroxide (0–100 mole%) were obtained by the coprecipitation method [5]. The mole % of aluminium hydroxide in the different samples (S1–S12) are: S1(0.00%); S2 (0.43%); S3 (0.76%); S4 (1.52%); S5 (2.06%); S6 (3.43%); S7 (8.33%); S8 (20.00%); S9 (40.00%); S10 (60.00%); S11 (80.00%) and S12 (100.00%). The hydroxides were dried at 110°C for 4 h and powdered samples of 350 BSS mesh size were used in the experiments reported here.

X-Ray diffraction patterns of the samples were obtained using a πPOH-I (U.S.S.R.) diffractometer consisting of a πPOH X-ray generator scintillation counter CPC-1-0 and counting and recording device CCII. The instrument was operated at 30 kV and 10 mA with a scanning rate of 1°C (2θ) min^{-1} for the analysis of phases and 0.25°C (2θ) min^{-1} for the determination of lattice parameters (accuracy ± 0.0002 Å). The source of radiation was Mn-filtered, FeK_α radiation ($\lambda = 1.947$ Å).

Thermal analyses were carried out in air using a derivatograph (MOM, Hungary) at a linear heating rate of 10°C min^{-1} with 120 mg samples in platinum crucible containers. Standard α-Al_2O_3 was taken as the reference material. The DTA and TG sensitivity, particle size, weight of the samples and the heating rate were kept constant throughout the measurements.

RESULTS AND DISCUSSION

DTA curves of pure ferric hydroxide (S1) and pure aluminium hydroxide (S12) are shown in Fig. 1. The endothermic peak at 170°C (50–320°C) in sample S1 is attributed to the removal of bound water molecules and the exothermic peak at 420°C (320–460°C) is due to the conversion of γ-Fe_2O_3 to α-Fe_2O_3 [9]. The broad endothermic peak (50–320°C) in the alumina gel (S12) when resolved consists of two endothermic peaks, i.e. the first peak appears at 120°C (50–220°C) and the second peak at 260°C (220–320°C). The first endothermic peak indicates the removal of bound water, whereas the second shows the removal of the constitutional water of hydrargellite [10–12]. Gels like aluminium hydroxide generally have large internal surfaces and are interwoven with capillaries of greatly varying sizes.

Because of capillary condensation and also colloidal forces, water from these gels can be removed from the inside material only at higher temperatures. This is probably the reason for the broad endothermic peak observed here. The endothermic peak at 420°C may be attributed to the conversion of bohemite to γ-alumina. Further, the TG results also support the presence of hydrated alumina gel $Al_2O_3 \cdot 3\ H_2O$ or 2 ($AlOOH \cdot H_2O$), bohemite (AlOOH) and alumina (Al_2O_3). Since the samples calcined at 110°C, 260°C, and 420°C are amorphous to X-rays, their structures could not be confirmed. However, the presence of γ-Al_2O_3 is indicated by electron diffraction studies on the sample S12, calcined at 420°C [13].

The differential thermal analysis curves of samples S1–S12 are given in Fig. 2.

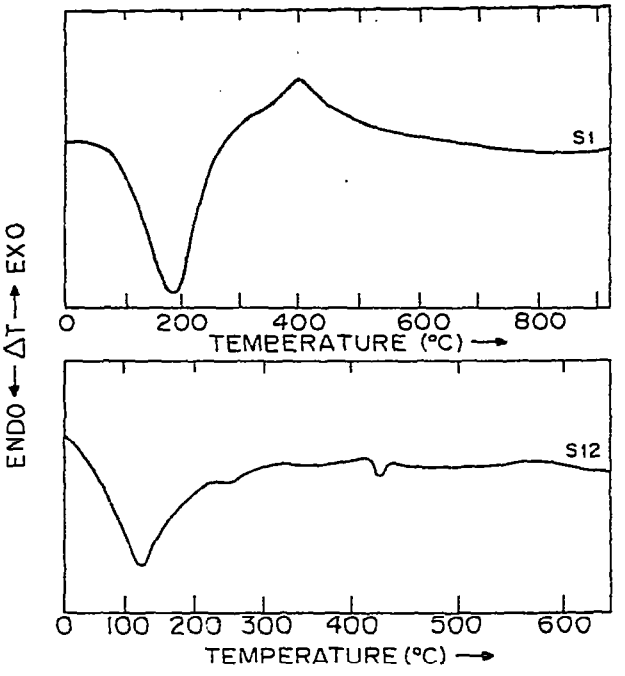

Fig. 1. DTA curves of ferric hydroxide (S1) and alumina gel (S12).

Table 1 shows the minima or maxima of the endo or exothermic peaks and corresponding temperature ranges. The DTA curves show three different regions: the first region (A) is below 240°C which is clearly shown by an endothermic peak;

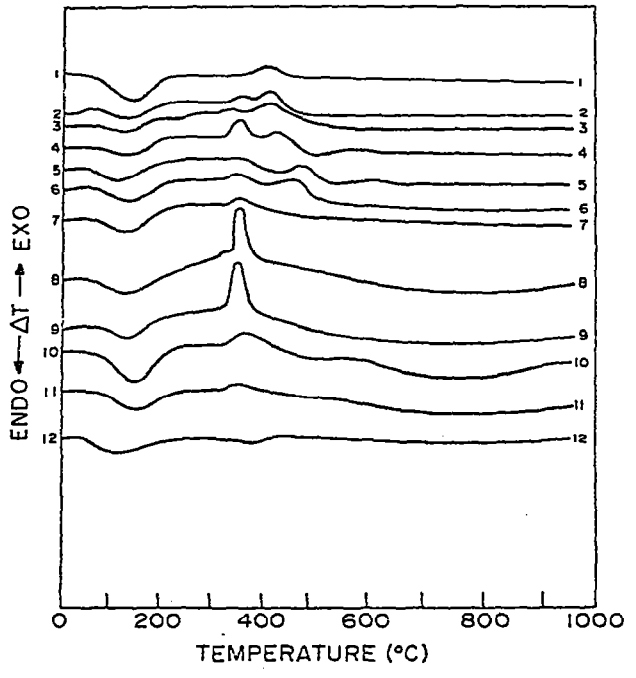

Fig. 2. DTA curves of iron(III)–aluminium(III) mixed hydroxide samples (S1–S12).

TABLE 1

Results of differential thermal analysis of iron–aluminium mixed hydroxide samples

Sample No.	Endothermic peak		Exothermic peaks			
	Peak temp. (°C)	Temp. range (°C)	First peak		Second peak	
			Peak temp. (°C)	Temp. range (°C)	Peak temp. (°C)	Temp. range (°C)
S1	170	80–220			410	320–460
S2	145	80–220	370	350–390	425	390–470
S3	145	80–200	340	335–365	425	380–475
S4	140	80–230	350	320–390	430	390–480
S5	140	90–210	360	340–380	490	440–530
S6	140	80–240	360	325–380	470	420–510
S7	140	80–230	365	350–380		
S8	130	80–230	360	300–410		
S9	140	80–230	360	300–400		
S10	150	80–230	365	330–400		
S11	145	80–240	355	320–380		
S12	150	80–315				

the second region (B) lies between 240 and 600°C, where one or more exothermic peaks are observed; and the third region (C) is beyond 600°C, where no such peaks are noticed. The endothermic peak around 140°C (80–240°C) shows the loss of bound water molecules.

There are two exothermic peaks in the DTA curves of samples S2–S6 in region B. One is at lower temperatures, i.e. around 360°C and the other is at higher temperatures, i.e. between 425 and 490°C. The intensity of the first exothermic peak gradually increases from S2 to S4 and then decreases up to S7. Samples S8 to S11 show only a single exothermic peak at 360°C, the intensity of which is maximum in samples S8 and S9, respectively. The two exothermic peaks in samples S2–S6 may be considered to arise from crystallization or a difference in particle size or the formation of a solid solution due to the interaction of the oxides at these lower temperatures.

Marel [14] and Kulf and Trites [15] observed that a decrease of particle size of minerals like goethite and meghamite lowers the peak temperature. According to Graf [16] and Kulf and Trites [15] the incorporatoin of iron into the structure of a mineral, substituting aluminium or magnesium, changes its intensity. But in the present case the intensity of the first exothermic peak varies with the concentration of alumina without practically affecting the peak temperature. Moreover, the specimens used here are of the same particle size. Hence it can be concluded that the impurity only influences the area of the peak.

The observed second endothermic peak in the range 425–490°C (Fig. 2) in samples S2–S6 can be explained as follows. The crystallization of α-iron oxide

occurs at 420°C in sample S1, and this may shift gradually to higher temperatures with the increase in concentration of alumina. Similar shifts in the exothermic peak were also observed by Bhattacharyya et al. [17] from 420 to 930°C in the mixed hydroxides containing 10–40 mole % of alumina, and they were attributed to the stabilization of iron oxide against crystallization. This was observed by Shirasaki et al. [18], i.e. from 500 to 650°C in the mixed hydroxides containing 15–33 mole % of alumina. The shift was ascribed to the combination state due to the interaction of these oxides at these temperatures. Similar behaviour is not observed in samples S7–S9 between 500 and 650°C. The occurrence of an exothermic peak at lower temperatures in the present study may be due to the method of preparation of these samples.

The exothermic peak at 360°C in samples S7–S11 may be due to either the substitution and stabilization of γ-alumina by iron oxide or the stabilization of iron oxide by alumina. Koehler [19] observed a sharp exothermic peak at 930°C in the specimen containing 2 mole % iron oxide in alumina obtained by coprecipitation of the mixed hydroxides. The exothermic peak was attributed to the stabilization of the crystallization of γ-alumina by iron oxide. Since no exothermic peak is observed above 600°C in these samples, the stabilization of iron oxide by alumina due to the interaction of these two oxides (since they are trivalent and similar ionic radii) may be the cause for the observed exothermic peak at 360°C.

The TG curves for different specimens are given in Figs. 3 and 4. Three different regions (A, B and C) as in the DTA curves can also be seen here. Regions A and C are only observed in the case of ferric hydroxide (S1), while all the three regions are present in pure aluminium hydroxide gel (S12). The portion concave to the *X*-axis in region B of the TG curve of sample S12 is very long and extends over a wider temperature range (220–580°C). This may be attributed to the removal of constitutional water molecules.

The loss in weight decreases around 140 to 240°C (as is seen from a rise in the curves in region A) as the aluminium concentration increases up to 1.50 mole % alumina (S4) and then increases gradually up to 8.33 mole % (S7). The decrease in loss of weight in the coprecipitated hydroxides up to sample S4 as seen in the TG curves and the increase thereafter may be attributed to the formation of a solid

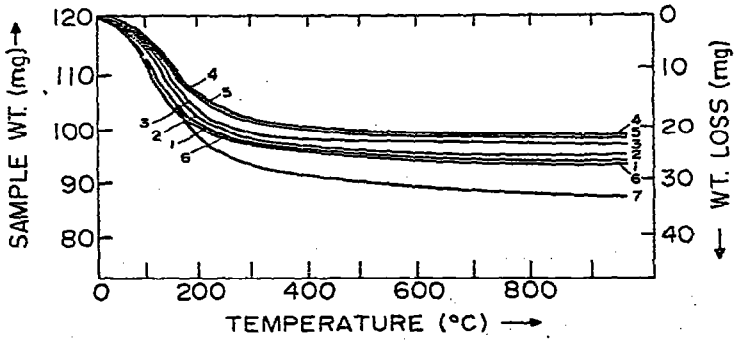

Fig. 3. TG curves of iron(III)–aluminium(III) mixed hydroxide samples (S1–S7).

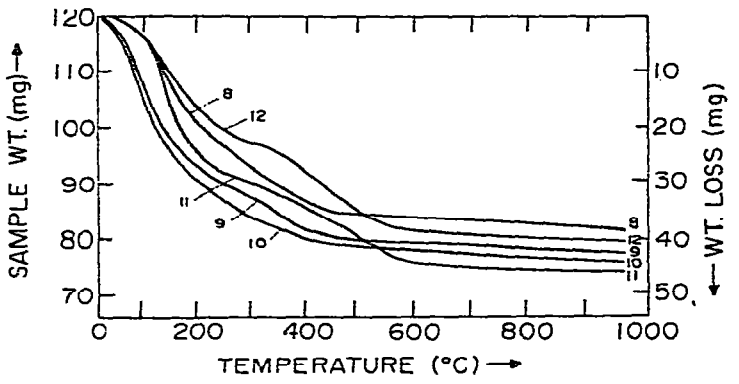

Fig. 4. TG curves of iron(III)–aluminium(III) mixed hydroxide samples (S8–S12).

solution due to the interaction of the two oxyhydroxides, which gives rise to a smaller weight loss in samples S2–S4 compared to that of either pure iron hydroxide (S1) or pure aluminium hydroxide (S12) at the same temperature. This conclusion is probably quite reasonable from the following point of view. A mutual interaction between the gels and the substitution of the cationic sites are common in the transition metal hydroxide gels as well as oxides, e.g. $Co(OH)_2$–$Mg(OH)_2$ systems observed by Matyshak et al. [20]. The substitution of Mg^{2+} ions by Co^{2+} ions in the gels gives TG curves which are not similar to those of pure cobalt hydroxide or magnesium hydroxide, and the temperature of dissociation also remains constant up to 12 mole % of $Co(OH)_2$. They attributed this to the interaction of the two specimens during their preparation. As these samples of iron–aluminium mixed hydroxide when heated below 240°C are amorphous to X-rays, the formation of a solid solution could not be confirmed. Similar behaviour of rise in the weight loss up to sample S4 and fall in the same afterwards is also observed in region C of the TG curves, where the oxides are present. It is possible that in the oxide region a similar interaction might be taking place.

To check the formation of a solid solution, X-ray analysis on samples S1–S12 calcined at 420°C were carried out. The mixed oxides containing 8.33 mole % are crystalline. However, the samples containing higher concentrations of alumina are amorphous to X-rays. A comparison of the *d*-values with the standard data indicates the presence of α-iron oxide in these samples. Shifting of the peak positions along with the splitting of the peaks and consequent change in lattice parameter confirm the formation of a solid solution even at this low temperature. The lattice parameter (Fig. 5) initially increases with increasing concentration of alumina up to about 1.5 mole %, then decreases up to 3.5 mole % and remains essentially unchanged thereafter. It has been explained earlier [5] that the increase is due to the formation of an interstitial solid solution and the decrease is due to the formation of a substitutional solid solution. In Fig. 5 the lattice parameter remains constant beyond 3.5 mole % due to the separation of excess alumina as the second phase.

The loss in weight of samples S8–S12 shows that it increases from samples S8 to

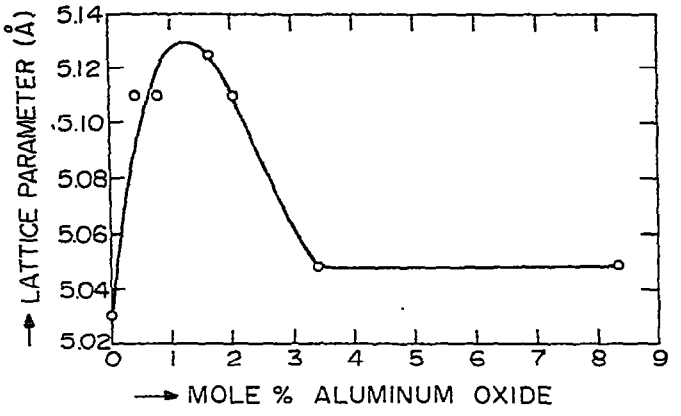

Fig. 5. Variation of lattice parameter with composition of alumina.

S10 and decreases thereafter in region A. This region is similar to the A region of the iron hydroxide gel (S1). Hence, the increase in loss of weight up to 60 mole % of alumina may be attributed to the formation of more zones enriched in hydrated iron oxide, while the decrease thereafter may be due to a decrease in the number of such zones. The B region in samples S8–S10, i.e. the section concave to the *X*-axis, is similar to the B region of the alumina gel (S12). The increase in loss of weight in this region for samples S8–S10 may be due to the formation of more and more zones enriched in aluminium oxyhydroxide, while the decrease thereafter may be due to a decrease in number of the same.

As samples S8–S12 calcined at 420°C are found to be amorphous to X-rays, no definite conclusion about the presence of zones and their structures can be made. However, electron microscopic and diffraction studies on these specimens explains the structural aspects as well as the presence of clusters in these samples, and the results will be published later [13]. The increase and decrease in the loss in weight of these samples in region C which contain only oxides can be explained in a similar manner. The TG curve shows that the length of the portions concave to the *X*-axis in region B increases in the curves of samples S8, S9, S11 and S12 while no such concavity is observed in sample S10. The concave portion in region A probably contains mainly zones enriched in hydrated iron oxide, while in region B it may be due to the zones enriched in aluminium oxyhydroxide, the extent of concavity being decided by the number of zones formed. The absence of a concave portion in sample S10 containing 60 mole % of alumina may be attributed to the interaction of the two zones with each other, which leads to a uniform distribution of the cations. A similar formation of zones in the cobalt–magnesium mixed hydroxide–oxide system was suggested by Matyshak et al. [20] from TG analysis.

CONCLUSIONS

The results of thermal analysis and X-ray diffraction studies of the iron–aluminium mixed hydroxide–oxide system clearly point to the formation of solid

solutions, i.e. the interstitial solid solution up to 1.5 mole % and substitutional solid solution up to 3.43 mole % and separation of excess alumina as the second phase thereafter. Samples containing more than 20 mole % of alumina probably contain zones enriched in either iron or aluminium oxyhydroxide depending upon the concentration of aluminium.

REFERENCES

1 H. Sato, A. Arrott and R. Kikuchi, J. Phys. Chem. Solids, 10 (1959) 19.
2 J.K. Srivastava and R.P. Sharma, Phys. Status Solidi B, 49 (1972) 135.
3 G. Haig, Philos. Mag., 2 (1957) 505.
4 B. Mani and V. Sitakara Rao, International Conference on the Applications of the Mössbauer Effect, Srinagar, J. and K., India, 13–17 July, 1981.
5 B. Mani and V. Sitakara Rao, J. Mater. Sci., 15 (1980) 925.
6 B. Mani and V. Sitakara Rao, React. Kinet. Catal. Lett., 13 (1980) 277.
7 R. Uma, M. Venkatachalam and J.C. Kuriocose, Proc. Int. Congr. Catal., North Holland Publishing Co., Amsterdam, 1972, pp. 11–245.
8 Krylov and Siyak, Neftekhimiya, 2 (1962) 688.
9 B. Mani and V. Sitakara Rao, Ind. J. Chemistry, 17 (A) (1979) 547.
10 L. Erdey and F. Paulik, Acta Chim. Eng. Hung., 7 (1955) 45.
11 Ibid., Acta Chim. Eng. Hung., 13 (1957) 117.
12 Z.D. Zivkovic, Thermochim. Acta, 21 (1977) 391.
13 B. Mani and V. Sitakara Rao, to be published.
14 H.W.V. Marel, Am. Mineral., 141 (1956) 222.
15 J.L. Kulf and A.F. Trites, Am. Mineral., 36 (1957) 23.
16 D.L. Graf, Am. Mineral., 30 (1951) 23.
17 S.K. Bhattacharyya, S. Kameswari and G. Srinivasan, Z. Phys. Chem., 214 (1960) 191.
18 T. Shirasaki, M. Okada, M. Uehara and K. Morikawa, Int. Chem. Eng., 7 (1967) 544.
19 E.K. Koehler, in R.F. Schwenker, Jr. and P.D. Garn (Eds.), Thermal Analysis, Vol. 2, Academic Press, New York, 1969, Vol. 2, p. 979.
20 V.A. Matyshak, M.Ya. Kushnev, M.P. Shibanov, A.A. Kadushin and O.V. Krylov, Kinet. Catal., 17 (2) (1976) 457.